RESEARCH REPORT

External Research Program

Moisture and Frost in Fiberglass Insulation (Second Report)

Canada

CMHC SCHL

HOME TO CANADIANS

CMHC—HOME TO CANADIANS

Canada Mortgage and Housing Corporation (CMHC) has been Canada's national housing agency for more than 60 years.

Together with other housing stakeholders, we help ensure that Canada maintains one of the best housing systems in the world. We are committed to helping Canadians access a wide choice of quality, affordable homes, while making vibrant, healthy communities and cities a reality across the country.

For more information, visit our website at **www.cmhc.ca**

You can also reach us by phone at 1-800-668-2642 or by fax at 1-800-245-9274.

Outside Canada call 613-748-2003 or fax to 613-748-2016.

Canada Mortgage and Housing Corporation supports the Government of Canada policy on access to information for people with disabilities. If you wish to obtain this publication in alternative formats, call 1-800-668-2642.

Moisture and Frost in Fiberglass Insulation

(Second Report)

By Robert W. Besant and Yong-Xin Tao

Department of Mechanical Engineering
University of Saskatchewan

30 April 1993

CMHC Project Manager: Tom Hamlin, Research Division

This project was carried out with the assistance of a grant from Canada Mortgage and Housing Corporation under the terms of the External Research Program (CMHC CR File 6585/B082-1). The views expressed are those of the authors and do not represent the official views of the Corporation.

Contents

List of Figures

List of Tables

ABSTRACT

An experimental procedure of measuring the heat of desorption and an analysis of the effect of thermal hysteresis on the transient heat and mass diffusion processes in fiberglass insulation were presented. The analysis incorporates the experimental results of the heats of sorption. The significance of thermal hysteresis and its interaction with dynamic heat and mass transport processes such as that a building insulation undergoes are investigated through experiments and a numerical simulation. An experimental apparatus that allows for the investigation of exfiltration and infiltration effects on the heat and moisture transport in insulation materials under the controlled test conditions was reported. The preliminary test results for exfiltration tests (winter conditions but excluding the buoyancy effects) were presented for a given temperature difference across a fiberglass test slab ($T_c = 20 \pm 1$ °C and T_∞=21 °C) at various air relative humidities (60 to 90 % RH) and two different exfiltration rates (1.66×10^{-4} and 2.49×10^{-4}m^3/s, or u_g = 1.0 and 1.5 mm/s). In this range, it is found that the increase in moisture accumulation under frosting condition could be an order of magnitude higher than for the temperature range above freezing. A one-dimensional numerical model predicted simultaneous heat transfer, vapor diffusion, convection, phase change and adsorption effects. Predicted results agree favorably with the measured data.

EXECUTIVE SUMMARY

This report summarizes the research results for a project under the External Research Contract, sponsored by CMHC, which continues the work initiated under a previous External Research Program project. The objectives stated in the original proposal – to measure the heats of adsorption and desorption, to correlate and include the measured data in numerical models, to modify the model to include air infiltration in fiberglass insulation, and to develop an experimental apparatus and plan tests to validate the modified model – have been accomplished during the period of the contract. Some of the important findings have been communicated to the appropriate scientific and engineering sectors through conference presentations and journal publications. In this report, the experimental study of measuring the heat of desorption is presented first. An analysis of the effect of thermal hysteresis on the transient heat and mass diffusion processes in fiberglass insulation follows. This analysis incorporates the experimental results of the heats of sorption. An experimental method that is used to study air infiltration/exfiltration effects in fiberglass insulation is then described, and the experimental results for temperature and moisture distributions under exfiltration conditions are presented. Finally, a transient, one- dimensional model for simultaneous heat and mass transfer with both phase changes and airflow (exfiltration effect) is presented, and the predictions are discussed and compared with the measured data.

Thermal hysteresis has been defined by the differences between the adsorption and desorption isotherms and between heats of adsorption and desorption. New data is presented for the desorption process which is contrasted with previously obtained adsorption data. The significance of this phenomenon and its interaction with dynamic heat and mass transport processes such as that a building insulation undergoes are investigated through experiments and a numerical simulation. From the measurement of heat of desorption reported here and data for the heat of adsorption, it is found that the thermal hysteresis phenomenon clearly exists for typical commercial fiberglass insulation. During transient processes thermal hysteresis effects are pronounced regardless of whether the insulation slab is initially dry or wet and above or below freezing temperature. Neglecting thermal hysteresis effects in simulating a dynamic transport process can lead to errors in the instantaneous heat flux of up to 51% for an initially dry fiberglass slab and 23% for an initially moist slab.

The preliminary test results for exfiltration tests (winter conditions but excluding the buoyancy effects) were presented for a given temperature difference across a fiberglass test slab ($T_c = 20 \pm 1$ °C and T_∞=21 °C) at various air relative humidities (60 to 90 % RH) and two different exfiltration rates (1.66×10^{-4} and 2.49×10^{-4}m^3/s, or $u_g = 1.0$ and 1.5 mm/s). In this range, it is found that the increase in moisture accumulation under frosting condition could be an order of magnitude higher than for the temperature range above freezing. A one-dimensional numerical model predicted simultaneous heat transfer, vapor diffusion, convection, phase change and adsorption effects. Predicted results agree favorably with the measured data.

Although this study has quantified the significance of each of several physical phenomena in fiberglass insulation and the size of errors that could result from the use of overly simplified models, much more work is required to investigate the behavior of fiberglass insulation under typical ranges of operating conditions.

«L'humidité et le givre dans l'isolant en fibre de verre»

Résumé

Ce rapport résume les résultats d'une recherche menée dans le cadre du Programme de subventions de recherche de la SCHL, laquelle poursuivait les travaux amorcés lors d'un contrat antérieur obtenu par l'entremise du même programme. Les objectifs fixés lors de la première proposition ont été atteints durant la période du contrat. Il s'agissait de mesurer la chaleur d'adsorption et de désorption, d'établir une corrélation parmi les données mesurées et de les intégrer à des modèles numériques, de modifier le modèle pour inclure l'infiltration d'air dans l'isolant en fibre de verre, de mettre au point un appareil expérimental et d'organiser des essais en vue de valider le modèle modifié. Certains résultats significatifs ont été communiqués aux scientifiques et aux ingénieurs intéressés au moyen d'allocutions dans des conférences et d'articles dans des revues spécialisées. Dans ce rapport, on présente d'abord l'étude expérimentale visant à mesurer la chaleur de désorption. Suit une analyse de l'effet de l'hystérésis thermique sur les procédés de chaleur transitoire et de diffusion de masse dans l'isolant en fibre de verre. Cette analyse incorpore les résultats expérimentaux des chaleurs de sorption. On décrit ensuite une méthode expérimentale servant à étudier les effets, sur l'isolant en fibre de verre, de l'infiltration et de l'exfiltration d'air ainsi que les résultats expérimentaux relatifs à la répartition de la température et de l'humidité dans des conditions d'exfiltration. Enfin, on présente un modèle unidimensionnel transitoire de transfert simultané de la masse et de la chaleur pour les changements de phase et le mouvement d'air (effet d'exfiltration) et on commente les prévisions en les comparant avec les données mesurées.

Par hystérésis thermique, on entend les différences qui existent entre les isothermes d'adsorption et de désorption ainsi qu'entre les chaleurs d'adsorption et de désorption. On présente de nouvelles données pour le procédé de désorption, lesquelles sont mises en contraste avec des données d'adsorption antérieures. L'importance de ce phénomène et son interaction avec les procédés de chaleur dynamique et de transport de la masse, comme ceux que subit l'isolation d'un bâtiment, sont examinés au moyen d'expériences et d'une simulation numérique. La chaleur de désorption mesurée et les données relatives à la chaleur d'adsorption permettent de conclure que l'hystérésis thermique est un phénomène qui touche véritablement l'isolant en fibre de verre commercial. Pendant les procédés transitoires, les effets de l'hystérésis thermique sont prononcés en dépit de l'état initial du matelas d'isolant (sec ou humide; au-dessus ou sous le point de congélation). Le fait de négliger les effets de l'hystérésis thermique dans la simulation du processus de transport dynamique peut entraîner des erreurs en ce qui a trait au flux de chaleur instantané pouvant atteindre 51 p. 100 pour un matelas d'isolant en fibre de verre sec à l'origine et 23 p. 100 pour un matelas d'isolant humide à l'origine.

Les résultats des essais d'exfiltration préliminaires (dans des conditions hivernales, mais sans tenir compte des effets de la poussée ascensionnelle) ont été présentés pour une différence de température donnée sur un matelas d'essai en fibre de verre (T_c = 20 ± 1 °C et T_∞ = 21 °C) à divers taux d'humidité relative (de 60 à 90 p. 100) et à deux taux d'exfiltration différents (1,66 x 10^{-4} et 2,49 x 10^{-4} m^3/s, ou μ_g = 1,0 et 1,5 mm/s). Pour ces valeurs, on s'aperçoit que l'augmentation de l'accumulation d'humidité en présence de givre pourrait s'avérer supérieure par un ordre de grandeur de 1 par rapport à l'échelle de température se situant au-dessus du point de congélation. Un modèle unidimensionnel numérique a prévu un transfert de chaleur, une diffusion de la vapeur, une convection, un changement de phase ainsi que des effets d'adsorption survenant simultanément. Les résultats prévus concordent avec les données mesurées.

Cette étude a certes quantifié l'importance de plusieurs phénomènes physiques propres à l'isolant en fibre de verre ainsi que l'ampleur des erreurs pouvant résulter de l'utilisation de modèles trop simplifiés, mais il faudra encore beaucoup d'autres études pour établir le comportement de l'isolant en fibre de verre dans des conditions variées, mais typiques, d'utilisation.

National Office
700 Montreal Road
Ottawa ON K1A 0P7
Telephone: (613) 748-2000

Bureau national
700 chemin de Montréal
Ottawa ON K1A 0P7
Téléphone : (613) 748-2000

Puisqu'on prévoit une demande restreinte pour ce document de recherche, seul le résumé a été traduit.

La SCHL fera traduire le document si la demande le justifie.

Pour nous aider à déterminer si la demande justifie que ce rapport soit traduit en français, veuillez remplir la partie ci-dessous et la retourner à l'adresse suivante :

Centre canadien de documentation sur l'habitation
Société canadienne d'hypothèques et de logement
700, chemin Montréal, bureau C1-200
Ottawa (Ontario)
K1A 0P7

Titre du rapport: _____

_____

Je préférerais que ce rapport soit disponible en français.

NOM _____

ADRESSE _____
rue App.

_____
ville province Code postal

No de téléphone ( ) _____

1 INTRODUCTION

This report summarizes the research results for a project under the External Research Contract, sponsored by CMHC, which continues the work initiated under a previous External Research Program project. The four objectives stated in the original proposal are:

1. To measure the heats of adsorption and desorption of typical fiberglass slabs under a range of ambient temperatures;

2. To correlate the measured data for the heats of adsorption and desorption for fiberglass and include these in theoretical/numerical models of fiberglass undergoing transient heat and mass diffusion processes with hysteresis effects;

3. To modify the one-dimensional theory for heat and mass diffusion through fiberglass to include air infiltration and use this transient, one-dimensional theory to develop a numerical model of transient heat and mass transfer with air infiltration through fiberglass insulation.

4. To develop an experimental apparatus and plan tests to validate the model for transient heat and mass transfer with air infiltration through fiberglass insulation.

The above-defined research objectives have been accomplished during the period of the contract. Some of the important findings have been communicated to the appropriate scientific and engineering sectors through conference presentations and journal publications [1-2]. In this report, we first present the experimental study of measuring the heat of desorption, followed by an analysis of the effect of thermal hysteresis on the transient heat and mass diffusion processes in fiberglass insulation. This analysis incorporates the experimental results of the heats of sorption. An experimental method that is used to study air infiltration/exfiltration effects in fiberglass insulation is then described, and the experimental results for temperature and moisture distributions under exfiltration conditions are presented. Finally, a transient, one-dimensional model for simultaneous heat and mass transfer with both phase changes and airflow (exfiltration effect) is presented, and the predictions are discussed and compared with the measured data. Although this study has quantified the significance of each of several physical phenomena in fiberglass insulation and the size of errors that could result from the use of overly simplified models, much more work is required to investigate the behavior of fiberglass insulation under typical ranges of operating conditions.

2 MEASUREMENT OF THE HEAT OF DESORPTION

The physical adsorption of a gas on a surface is accompanied by the release of thermal energy; conversely, the physical desorption of a gas from a solid surface requires the addition of thermal energy. These heats of sorption are defined by the initial and final thermodynamic states of the system and the conditions under which any heat flux takes place; examples are adiabatic heat of sorption, isosteric heat of sorption, etc. [3]. In engineering related problems

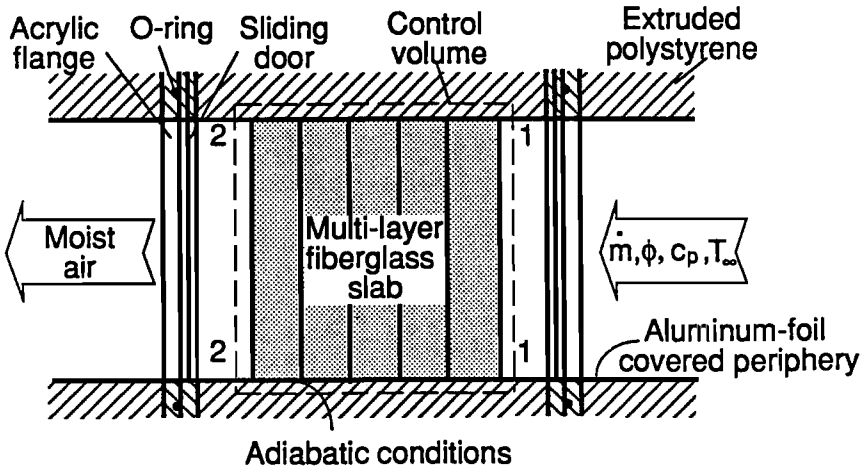

Figure 1: The test section. Indicated also is the control volume for the derivation of the measurement principle.

the most common sorption process is isosteric. In thermodynamic terms, the isosteric heat of sorption is the differential enthalpy of sorption which can be used in solving the differential energy equation (as compared to the definition of integral enthalpy of sorption). In general, the isosteric heat of sorption at a given ambient pressure has the following functional form,

$$h_{\text{sorp}} = f(W, T, \text{adsorptive gas, adsorbent solid}), \tag{1}$$

where W is the equilibrium content of adsorbate and T is the absolute temperature. Because W is a function of temperature T and relative humidity ϕ for a given sorptive-sorbent system, equation (1) can be written as,

$$h_{\text{sorp}} = f(\phi, T). \tag{2}$$

Due to the hysteresis in sorption isotherms, the heat of adsorption, for a given system, may not have the same functional form as that for heat of desorption. This might be explained at a molecular level. Physical sorption results in a monolayer or a few layers of adsorbate molecules that are attached to the solid surface. Different equilibrium adsorbate mass after adsorption or desorption implies different levels of interaction forces between adsorbate molecules and between adsorbate and solid molecules. As a result of this, the amount of energy required to break the molecular bonds during desorption would not necessarily be the same as the adhesive energy released during adsorption. In practice, however, other factors such as surface contamination change the sorbent surface characteristics and further enhance the irreversibility in energy exchange for sorption processes.

2.1 Experimental Method

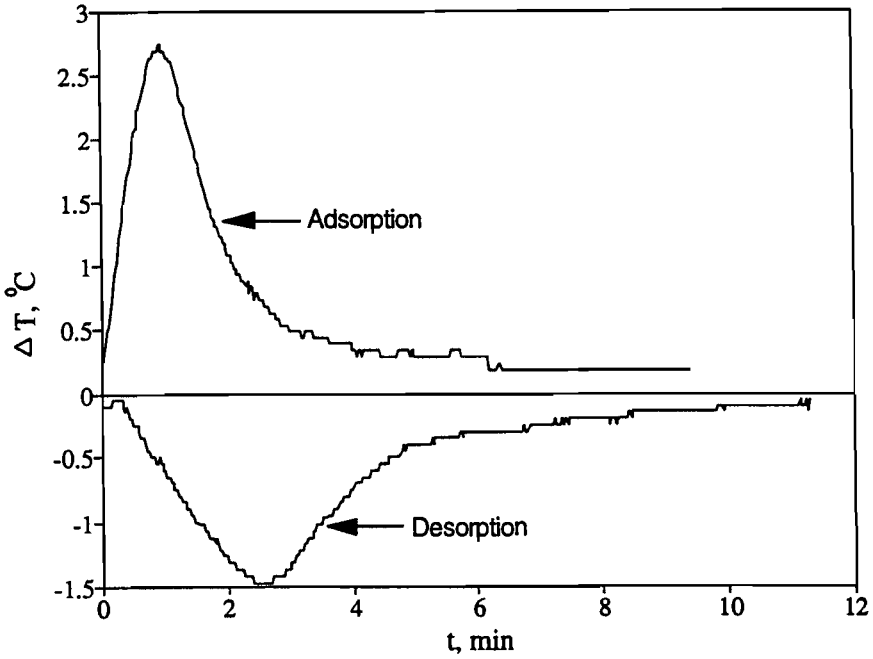

Figure 2: Typical time variation of the experimental temperature difference $\Delta T = T_2 - T_1$ for $\rho = 71.2$ kg/m^3.

A simple and practical method developed by Tao et al. [4] is used to measure both heat of adsorption and heat of desorption for a typical, medium-density fiberglass slab. The control volume, shown in Fig. 1, consists of an insulation matrix which undergoes an adsorption or desorption process. Initially the control volume which contains the insulation test sample is at an uniform temperature, T_o, and relative humidity, ϕ_o. At time $t = 0^+$, air at a controlled temperature, T_∞, and humidity, ϕ_∞ flows through the sample. To minimize any heat fluxes, except due to sorption within the test sample, T_o is set to be equal to T_∞ or T_1. As the air passes through the sample adsorption or desorption takes place. This causes the air temperature leaving the control volume (T2) to change relative to the inlet temperature (T1) (Fig. 1). In the case of adsorption, thermal energy is released to the air which is passing through the test sample at a controlled rate therefore temperature (T2) rises, while for desorption this temperature decreases. When the adsorption/desorption process is completed the test sample is again in thermodynamic equilibrium with the surroundings at T_∞ and ϕ_∞. Applying the first law of thermodynamics and conservation of mass for a constant air mass flow rate ($\dot{m}_a$) and a constant specific heat of air (c_{pa}) the average heat of adsorption/desorption is [4],

$$\bar{h}_{\text{sorp}} = \frac{c_{\text{pa}}\dot{m}_a S}{\Delta m}, \tag{3}$$

where $\bar{h}_{\text{sorp}}$ is the average heat of adsorption/desorption , Δm is the mass of water vapor adsorbed/desorbed and

$$S = \int_0^t (T_2 - T_1)dt \tag{4}$$

is the temperature signature (Fig. 2) and is determined using numerical trapezoidal integration.

It should be noted that the average heat of sorption, as in equation (3), from some initial state temperature, T_∞, and relative humidity, ϕ_o, to a final state of T_∞ and ϕ_∞ is not the same as the heat released/absorbed at any intermediate state. To get the thermodynamic state heat of adsorption/desorption, we can write the average heat of adsorption/desorption as a function of adsorbed/desorbed water vapor, W, by choosing a proper correlation,

$$\bar{h}_{\text{sorp}} = f(W, T_\infty), \tag{5}$$

so that for a given T_∞ we can write the thermodynamic heat of sorption as

$$h_{\text{sorp}}(W) = \frac{\partial W \bar{h}_{\text{sorp}}}{\partial W} = \bar{h}_{\text{sorp}} + W \frac{\partial \bar{h}_{\text{sorp}}}{\partial W}, \tag{6}$$

where, by definition

$$\bar{h}_{\text{sorp}} = \frac{1}{W} \int_0^W h_{\text{sorp}} dW. \tag{7}$$

From a thermodynamic point of view, the above-defined average heat of sorption has a reference point at zero vapor pressure corresponding to a zero relative humidity. This condition is very difficult to be controlled by the present experiment. As shown later, all the measured data for W and h' are based on the reference state of T_∞ and $2 < \phi < 4\%$. For slight variations in the reference state, we need only to use a transformation of $W = W^* - W_o$ where W^* is the absolute mass of adsorbate with respect to the vacuum state and W_o is the residual mass of adsorbate at $0 < \phi < 5\%$ such that equations (6) and (7) are still the valid representations of the heats of sorption for practical situations. Therefore, from the measured average heat of sorption (equation (3)), the thermodynamic state heat of sorption can be found using equation (6). For comparison with heat of vaporization, the results will be presented as a ratio of the heat of adsorption/desorption to heat of evaporation. That is,

$$h' = \frac{h_{\text{sorp}}}{h_{\text{fg}}} \text{ or } \bar{h}' = \frac{\bar{h}_{\text{sorp}}}{h_{\text{fg}}}. \tag{8}$$

where h' refers to the latent heat ratio and h_{fg} is the heat of evaporation.

The schematic of the apparatus is shown in Fig. 3. The sample is initially moist and the air is dry. The insulation is humidified with air from an air bath loop. After the initial thermal and mass equilibrium condition is reached, the sample is weighed. The test begins by opening the upstream and downstream sliding doors (see Fig. 3) and using the vacuum pump to draw air through the sample (see Fig. 3). The dry air is drawn from a large plastic bag filled with dry air at ambient pressure. The air in the plastic bag is dried with a desiccant drying loop which provides air humidities below 5% relative humidity. The mass flow rate of air is measured with the orifice plate and the computer data acquisition unit continuously records the temperature of all three thermocouples. Initially the temperature at the downstream thermocouple (TC2), shown in Fig. 3, changes as desorption occurs. When the temperature of TC2 returns to that of TC1 the equilibrium is accomplished and the test is stopped by closing the sliding doors. The final mass of the sample is then measured and the average heat of sorption is found using equation (3).

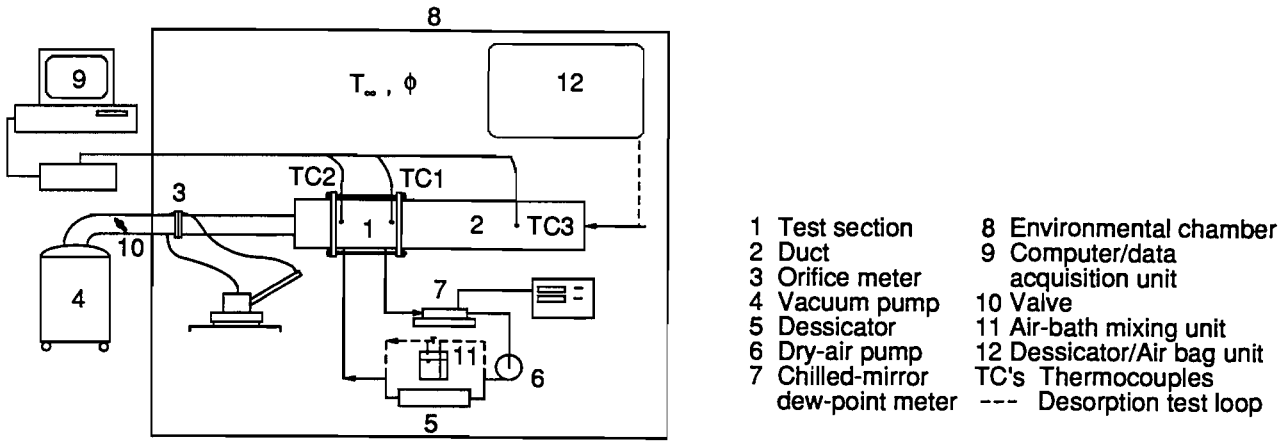

Figure 3: The schematic of the apparatus.

The overall system error for measured heat of sorption is 10% and the random error or repeatability is normally within ±15% [4].

2.2 Heat of desorption

The measured average heat of desorption is shown in Fig. 4, plotted as $\bar{h}'$ versus W, where W is the mass percent of vapor adsorbed/desorbed defined as

$$W = \frac{\Delta m}{m} \times 100 \tag{9}$$

where m is the total mass of dry sample. For comparison, the heat of adsorption is also plotted. It can be seen that $\bar{h}'$ is always greater than unity and is larger for low W (as expected). Physically, low W values correspond to the case where only a single molecular layer is being adsorbed or desorbed from the insulation fibers. The bonding forces between the fibers and the water molecules therefore prevail, and are stronger than those between water molecules; hence, more energy is needed to break the bond during desorption (and vice versa during adsorption) at low W. As the mass adsorbed/desorbed is increased there are many layers of water vapor molecules on the fiber, and as a result the bonding is basically between water molecules, resulting in a lower enthalpy of sorption.

The following correlations for the average and differential heat of desorption are found by fitting a cubic polynomial to the experimental data. They are:

$$\bar{h}' = 9.218 - 118.344W + 570.428W^2 - 883.76W^3, \ 0 \leq W \leq 0.18\%, \tag{10}$$

$$\bar{h}' = 1.58 - 1.87W, \ 0.18 < W \leq 0.31\%, \tag{11}$$

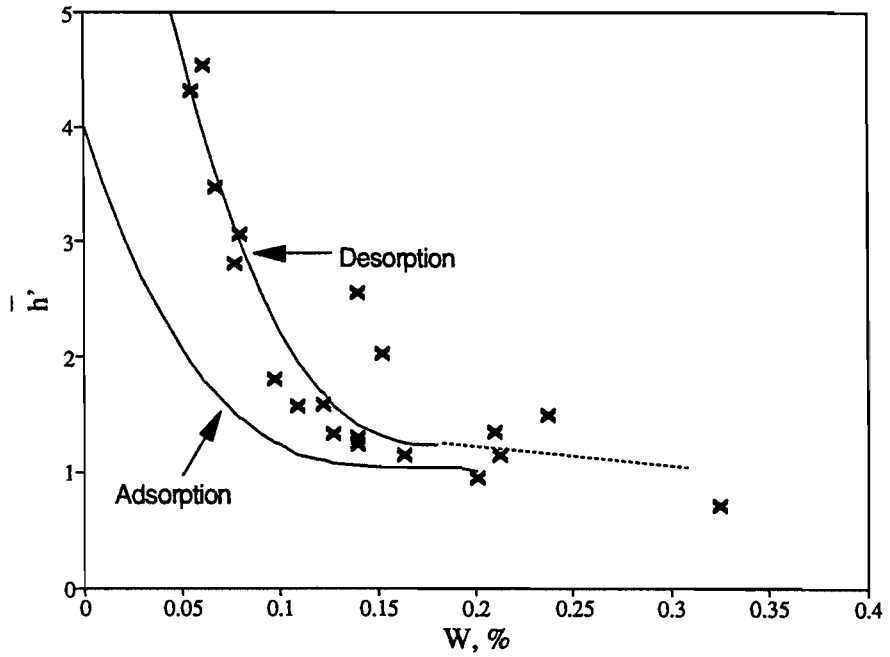

Figure 4: The ratio of the average heats of desorption (and adsorption) to the heat of vaporization as a function of W, %.

$$h' = 9.218 - 236.688W + 1711.284W^2 - 3535.944W^3, \quad 0 \leq W \leq 0.052\%, \tag{12}$$

$$\bar{h}' = 1, \quad W > 0.31\%, \text{ and } h' = 1, \quad W > 0.052\%. \tag{13}$$

These results, obtained at a temperature of 20°C, can be applied to a range from 5°C to 30°C [4]. The results in [4] show that the heat of adsorption is independent of temperature in the range of 5°C to 30°C because such a change is small on the absolute temperature scale. The same is assumed to apply to desorption. Like adsorption, the heat of desorption is independent of the porosity and permeability of the fibrous sample because the heat of desorption as defined in this paper is a specific quantity; therefore, the above correlations apply for insulation with a density of 54.3 - 71.2 kg/m^3 [4]. Although the measurement uncertainty was estimated to be ±15% the expected error in these correlations due to curve fitting is much smaller. (Initially it was hoped to carry out adsorption and desorption tests over an even wider range of temperature conditions. This was not possible without very expensive modifications to the experimental setup. Nonetheless, because the heats of adsorption and desorption were shown to be somewhat independent of temperature within the range of tests, it is expected that they will not differ substantially over even larger temperature ranges than those tested in this study.)

The differential or thermodynamic state heats of adsorption and desorption are plotted together in Fig. 5. These graphs again show the thermal hysteresis effect when water vapor is adsorbed/desorbed in fiberglass insulation. Also plotted in Fig. 5 is the reported isosteric heat of desorption [4] which was derived from the desorption isotherms reported in ref. [5] (for a uniform abscissa scale a continuous curve connects the isothermal data). A large discrepancy is obvious between the measured heat of desorption and that determined from isothermal sorption data. This indicates that the only reliable way to determine the heat of adsorption/desorption for a given sorptive sorbent system is to measure them directly

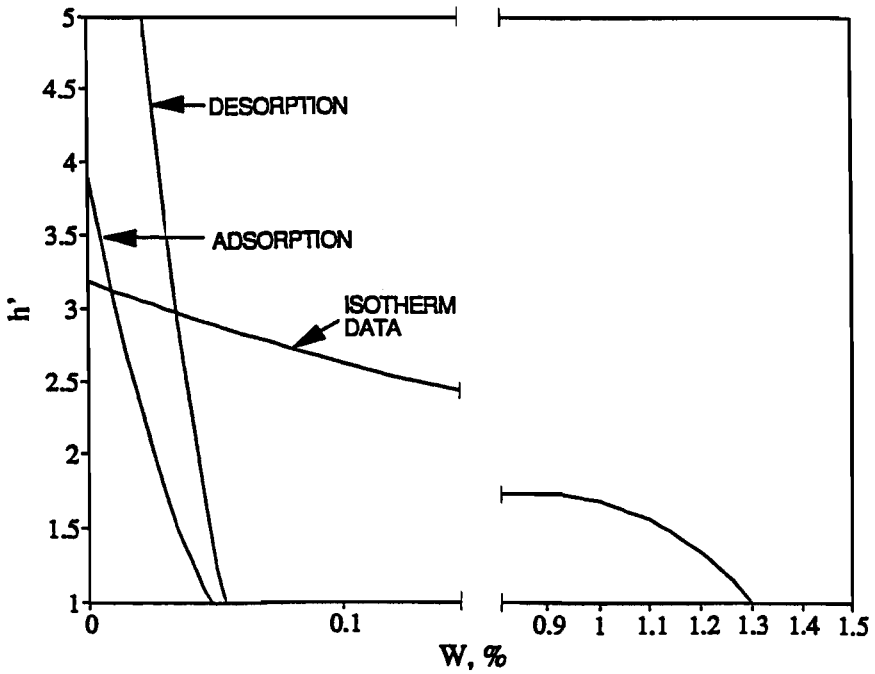

Figure 5: Comparison of the differential heats of adsorption and desorption.

with an appropriate experiment. The experimental method used in this paper should be representative of that which occurs due to infiltration/exfiltration in an insulated building envelope and as a result should be an accurate indication of the thermal hysteresis effects occurring in many fibrous insulation in service.

2.3 Thermal Hysteresis

Commercial fiberglass insulation (batts or loose fills) has a different equilibrium adsorbate mass exposed to air at a particular temperature and humidity after undergoing an adsorption or desorption process. This mass sorption hysteresis phenomenon, as will be analyzed later, is characterized by two different isotherms, (the relation between the equilibrium adsorbate mass and partial pressure, or relative humidity, of the adsorptive gas) and is also accompanied by two different energy exchange capacities or heats of adsorption and desorption. Physically the hysteresis in mass transfer and heat transfer occur concurrently; mass transfer could be measured separately but the heats of sorption measurement requires both heat and mass transfer data. Therefore, we can combine the hysteresis in mass transfer and heat transfer into a so- called 'thermal hysteresis' phenomenon.

Thermal hysteresis, defined in this study, is a phenomenon that results from the coupling between mass transfer and heat exchange capacity due to adsorption and desorption. It has two characteristic elements: the hysteresis in the adsorption and desorption isotherms and the hysteresis in the adsorption and desorption energy per unit mass of adsorbate, usually called heats of adsorption and desorption.

The hysteresis in equilibrium mass of adsorbate has been known for many hygroscopic

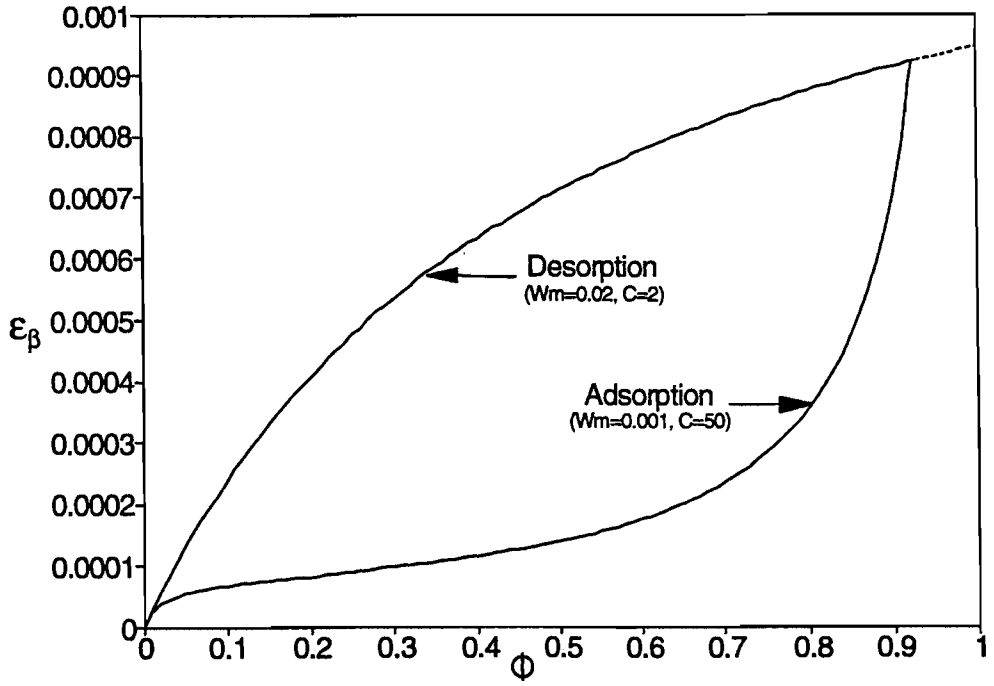

Figure 6: Typical adsorption and desorption isotherms for fiberglass insulation [1,4].

materials such as wood, cotton, etc. For fiberglass materials, several experimental isotherms, as summarized in ref. [5], clearly show a strong hysteresis effect. From these data sets, it can be reasonably assumed that for a medium dry-density fiberglass batt, the adsorption isotherm exhibits a trend that can be approximated by the BET equation,

$$W/W_m = \frac{C\phi}{[1-\phi][1+(C-1)\phi]}, \tag{14}$$

while the desorption isotherm follows the Langmuir equation

$$W/W_m = \frac{C\phi}{1+C\phi}, \tag{15}$$

where W_m and C are empirical constants and also $W = \epsilon_\beta \frac{\rho_\beta}{\rho_o}$.

Figure 6 shows a typical hysteresis loop of adsorption and desorption isotherms for fiberglass insulation. For a given relative humidity ($0< \phi <90\%$), the equilibrium mass for adsorption is smaller than that for desorption. This is primarily due to capillary effects which arises in porous materials with a large pore-size distribution [2]. Fiberglass insulation has a significant pore size variation due to a somewhat random distribution of fibers. It should be mentioned that hysteresis in the isotherms shown in Fig. 6 does not mean that fiberglass insulation is highly hygroscopic. Compared to other hygroscopic materials, the magnitude of adsorbate mass in fiberglass insulation is much smaller. As will be shown later, having small physical sorption capacity does not prevent fiberglass insulation from exhibiting strong thermal hysteresis effects.

Thermal hysteresis is also evident in the average heats of adsorption and desorption shown in Fig. 4. The curves are similar in that the heats of adsorption and desorption are

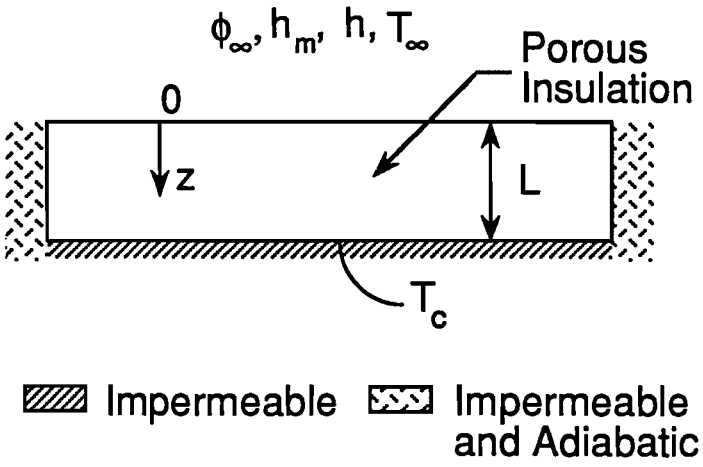

Figure 7: Schematic diagram of an insulation slab subject to a cold plate on one side and warm moist air on the other.

many times greater than the heat of vaporization for low values of W. Also, both curves approach the heat of vaporization for larger values of W. The curves are different in that the heat of desorption is always greater than the heat of adsorption and particularly for low values of W. For example, the first experimental data point for desorption is $\bar{h}'$=4.5 for $W = 0.06\%$ which is 150% greater than that for adsorption ($\bar{h}'$=1.8 at $W = 0.06\%$). Clearly this hysteresis effect may be significant when adsorption and desorption occur simultaneously in different regions of fiberglass insulation.

3 NUMERICAL MODEL WITH THERMAL HYSTERESIS EFFECTS

3.1 Theoretical Background

Given the evidence of hysteresis phenomena in adsorption and desorption isotherms and the measured heats of adsorption and desorption, it is important to investigate the magnitude of their effect during typical transient heat and mass transfer processes in an insulation slab. A numerical study is, therefore, presented to quantify this thermal hysteresis effect.

The simultaneous heat and mass transfer problem studied is one-dimensional and transient and is formulated using the local volume averaging technique [5]. Figure 7 is a schematic diagram of the physical configuration of the problem. The fiberglass slab is exposed to warm moist air on one side and a cold plate on the other. No convection (neither natural nor forced convection) from the gaseous phase is considered; therefore, vapor diffusion is the only mode for the moisture transport, and phase changes are caused by evaporation/condensation, sub-

Table 1: Physical Data of the Samples

ρ, kg/m^3	54.3	71.2
τ, %	6.7	7.8
d, μm	10	10

limation/ablimation and adsorption/desorption. This treatment is considered in order to isolate the convective effects from the hygroscopic effect and to identify the significance of the hygroscopic hysteresis effect compared to bulk phase changes during moisture transport in insulation. Detailed discussions on the numerical technique used can be found elsewhere [5]. The governing equations and other relations used in the formulation are listed in the Appendix. Also included in the Appendix are the initial conditions and boundary conditions used in this study.

During adsorption and desorption the relative humidity is below 100% and the Clapeyron equation cannot be used to describe the relation between the vapor pressure and temperature. If we assume that the time scale required to reach sorption equilibrium at local sorption sites is of the same order of the time scale for local thermal equilibrium, then the supplementary equations describing the equilibrium adsorption and desorption masses and the heats of sorption under thermodynamic equilibrium can be used in conjunction with the governing equations that describe a dynamic transport process. The typical sorption isotherms, shown in Fig. 5, and the appropriate differential heats of adsorption and desorption, shown in Fig. 6, are employed in the numerical calculation. It is further assumed that the relation for h' could be extrapolated to the below freezing temperature range such that h' represents the ratio of heat of sorption to the heat of sublimation. This assumption is based on the observation that the $h' - W$ relation is not very sensitive to the absolute temperature. The formulation is then complete. It should be noted that in Fig. 5 the adsorption and desorption isotherms intersect at $\phi = 92.3\%$. In the numerical model, the desorption curve (broken line in Fig. 5) is used for both adsorption and desorption when the relative humidity is greater than 92.3 %.

The physical data used in this study is listed in Table 1. To avoid further complication, frost accumulation on the cold surface is not included as a special boundary condition even though experimental evidence shows it to be important [6].

3.2 Numerical Results

In this study two cases are examined using the physical model in Fig. 7, case 1 where dry insulation undergoes wetting and case 2 where an initially moist insulation slab is being dried. In case 1, the insulation is initially dry ($\phi_o = 10^7$) and at room temperature, T_∞, when it is subject to very moist air (ϕ_∞=0.97) on the warm side ($z = 0$) and a cold plate (T_c) at$z = L$. During this process, adsorption is the dominant mode for local phase change

for a large portion of the insulation slab, and due to the initially low moisture content of the insulation thermal hysteresis effects are expected to be significant during the transient period. For case 2, the slab initially contains room temperature air at a high local relative humidity ($\phi_o = 0.8$) when it is exposed to a lower ambient relative humidity (ϕ_∞=0.4) on the warm side ($z = 0$) and temperature, T_c, at $z = L$. In this case desorption prevails at the places near the warm side of the slab but, due to the high moisture content of the insulation, the heats of adsorption and desorption nearly equal the heat of evaporation (or heat of sublimation when the local temperature falls below the freezing point). The effect of the cold plate temperature is addressed by testing both cases for cold plate temperatures well below freezing, 252 K, and slightly above freezing, 278 K.

A transition Fourier number ($\mathrm{Fo_{tr}}$) can be used to characterize the hygroscopic effects of a fiberglass insulation [5] and is defined as the dimensionless time when the local air relative humidity at $z/L = 0.9$ is greater than 90%. The transition Fourier number characterizes the commencement of the quasi-steady state in which hygroscopic effects are negligible although capillary effects are still present. Figure 8(a) shows Fo_{tr} for cases 1 and 2 when the plate temperature is 252 K. It is observed that Fo_{tr}, for an initially dry slab, is much larger than that for an initially wet slab. In Fig. 8(b), the results for T_c=278 K (i.e., no frosting effects) are shown. In this case, Fo_{tr} is slightly larger than that for a sub- freezing cold plate temperature. The results for which no hygroscopic, thermal hysteresis effects are used are also shown as the broken lines in Fig. 8. For no hysteresis effects, only one of the sorption isotherms and one of the heats of sorption are used. Equation (15) is used in case 1 where adsorption is expected to predominate, and equation (14) is used in case 2 where desorption should prevail. The heat of desorption is used for case 1 but the heat of adsorption for case 2. These selections are made to illustrate the consequence of neglecting thermal hysteresis effects in modeling typical drying or wetting processes. Figure 8 shows very different results when hysteresis effects are altered for the initially dry sample case 1 by using only the desorption isotherm equation (15) in place of the correct adsorption equation (14). The relative humidity curves for air in Fig. 8 for case 1 closely resemble the adsorption and desorption volume fraction curves in Fig. 5 because this process appears to be dominated by molecular diffusion in the interstitial space of the fibrous insulation and the hygroscopic adsorption process up to the transition Fourier numbers, Fo_{tr}.

The effect of the cold plate temperature in Fig. 8 (a) and (b) does not cause much change in the air relative humidity for the case of the initially dry sample (case 1) but it does have a large effect on Fo_{tr} for case 2 with an initially moist fiberglass slab. In Fig. 8 (b), Fo_{tr} at 0.8 corresponds to a 3.56 hour hygroscopic time period for the problem under investigation. A hygroscopic time period this large would imply that steady state conditions may not exist in typical fibrous insulation systems used in many building envelopes subject to large diurnal variations in temperature and humidity.

Figure 9 shows the heat-flux ratio Q' as a function of Fo. This heat transfer ratio is defined at the cold side of the insulation as the ratio of heat flux for the specified dynamic process to that for a completely dry slab under the same temperature boundary conditions (see Appendix equation (48)). These heat flux ratios can be significantly greater than unity.

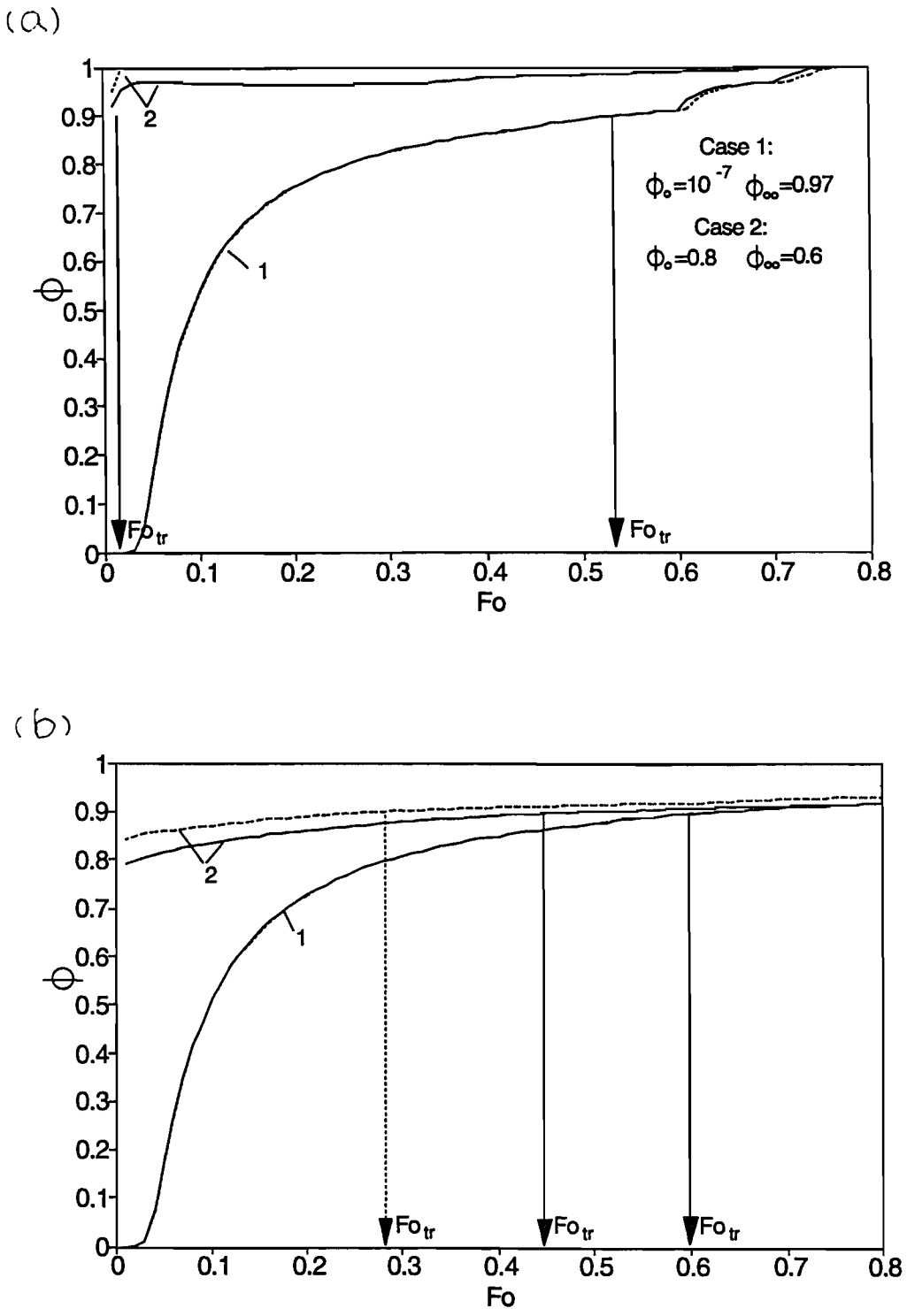

Figure 8: Time variation of the local relative humidity at $z = 0.9$ indicating a transition Fourier number for (a) $T_c = 252$ K and (b) $T_c = 278$ K. The broken lines correspond to the results assuming no thermal hysteresis effects.

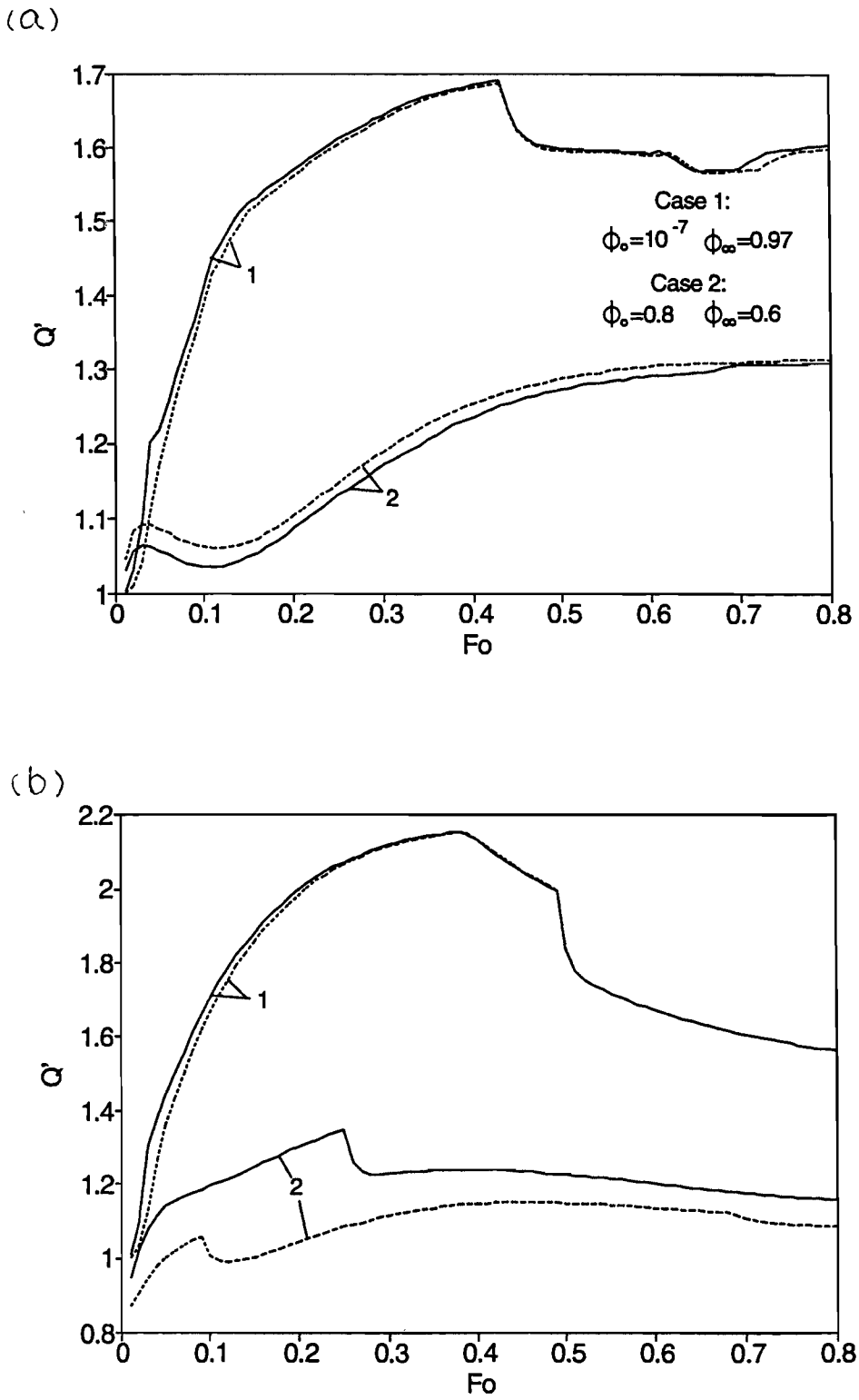

Figure 9: Time variation of the heat-flux ratio for (a) $T_c = 252$ K and (b) $T_c = 278$ K. The broken lines correspond to the results assuming no thermal hysteresis effects.

Once again, the broken lines in Fig. 9 are for the case where the hysteresis effects are neglected using the assumptions outlined above. When thermal hysteresis is neglected for an initially dry fiberglass slab (case 1) Q' is greatly overestimated for both 252 K (Fig. 9(a)) and 278 K (Fig. 9(b)). The maximum difference in these instantaneous heat flux ratios at $z = L$ is 51% at Fo=0.53 in Fig. 9(b). The heat flux error introduced by neglecting hysteresis in adsorption and desorption for an initially moist slab (case 2) is much smaller, especially for a sub-freezing cold plate temperature (Fig. 9(a)). The maximum heat flux difference at $z = L$ introduced by neglecting this hysteresis is 23% at Fo=0.2 which is reduced to 6% at Fo=0.8 for quasi-steady state (Fig. 9(b)).

To further demonstrate hysteresis effects, the rate of phase change, $\dot{m}$, at $z = L$ ($\dot{m} < 0$ means adsorption, condensation or ablimation and $\dot{m} > 0$ implies desorption, evaporation or sublimation) is presented for cases 1 and 2 in Figs. 10 (a) and (b), respectively. Neglecting thermal hysteresis may result in a different prediction of the mass accumulation and heat flux at $z = L$. As shown in Fig. 10 the rate of phase change (dimensionless) at the cold plate, including thermal hysteresis effects, is very different from that neglecting thermal hysteresis. Because the heat flux at $z = L$ depends on the phase change at $z = L$ and throughout the insulation slab, the difference in the predicted $\dot{m}$ clearly explains the difference in Q' shown in Fig. 9.

4 EXPERIMENTAL STUDY OF HEAT AND MOISTURE TRANSPORT WITH EXFILTRATION IN INSULATION

4.1 Experimental Apparatus

The schematic of the apparatus is shown in Fig. 11. A four layer glass-fiber slab (AF545, Fiberglas Canada, ON) with a total dimension of 275 × 600 × 95 mm, is placed in a test section. At the bottom of the test section is a cold plate which can be cooled well below the triple point temperature of water through a heat exchanger. A small air gap exists between the bottom surface of the insulation slab and the cold plate to allow for the exfiltration or infiltration of air through the insulation slab. An ethylene glycol-water solution is used as a heat exchanger coolant and is supplied by a pump from a storage tank which is placed in an environmental chamber. On top of the cold plate is mounted a heat-flux meter which allows for the measurement of the heat flux through the cold plate assembly. This measurement is used in the calculation of the heat flux through the insulation slab. The heat-flux meter consists of a polyethylene sheet with a 1/8 inch (3.175 mm) thickness and 21 thermocouples at each side of the sheet. An aluminum sheet with a 1/8 inch thickness is mounted on the top of the polyethylene sheet to keep the top surface temperature uniform. The thermal conductance ($W/m^2\ ^oC$) of the heat-flux meter is calibrated *in situ* using a heat-flow transducer. Another 10 thermocouples are placed between the glass fiber layers and on the exposed top and bottom surfaces of the slab to allow for the recording of the temperature

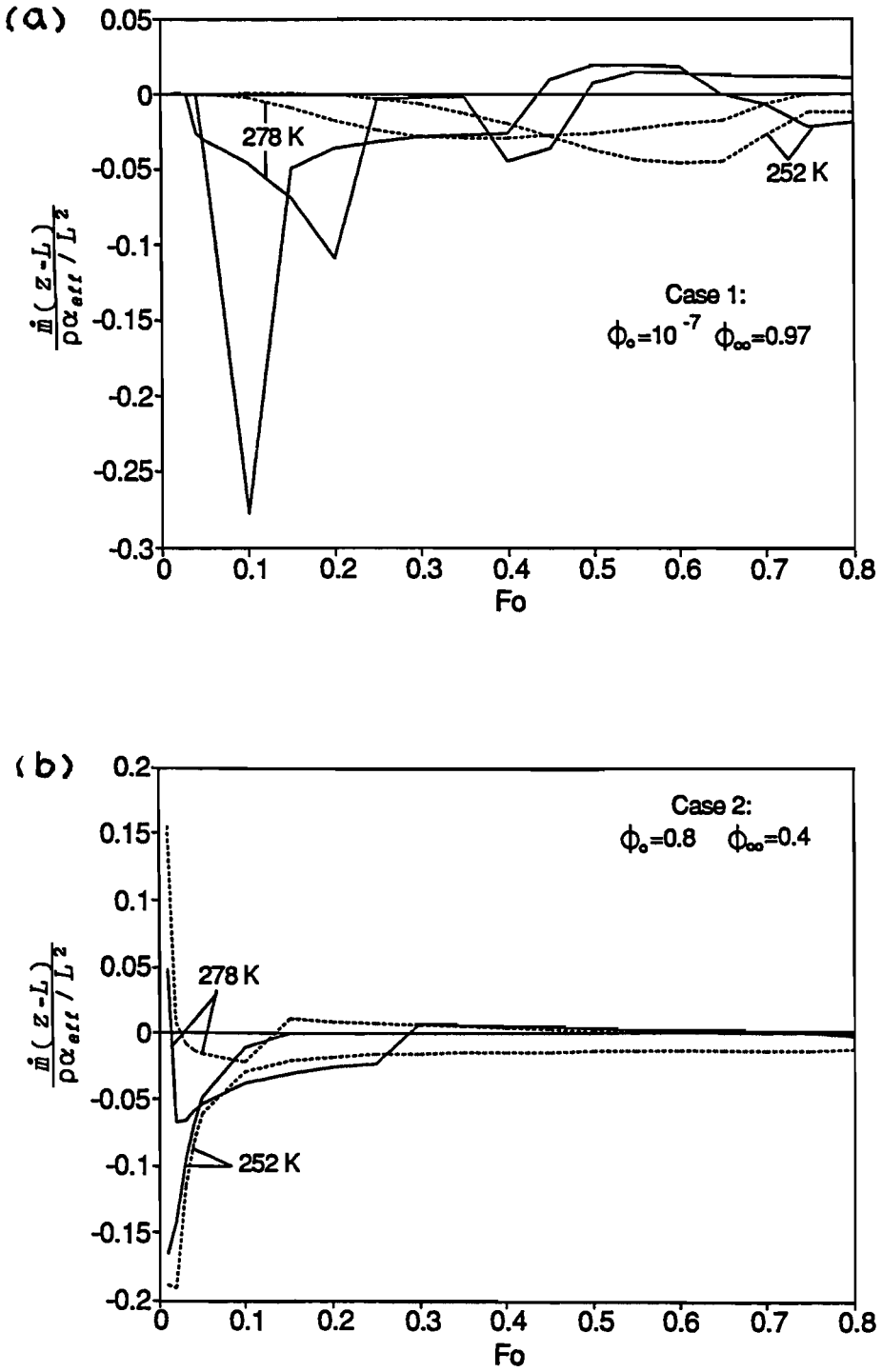

Figure 10: Rate of phase change at the cold plate ($z = L$) for (a) case 1 and (b) case 2 at two different cold temperatures. The broken lines correspond to the results assuming no thermal hysteresis effects.

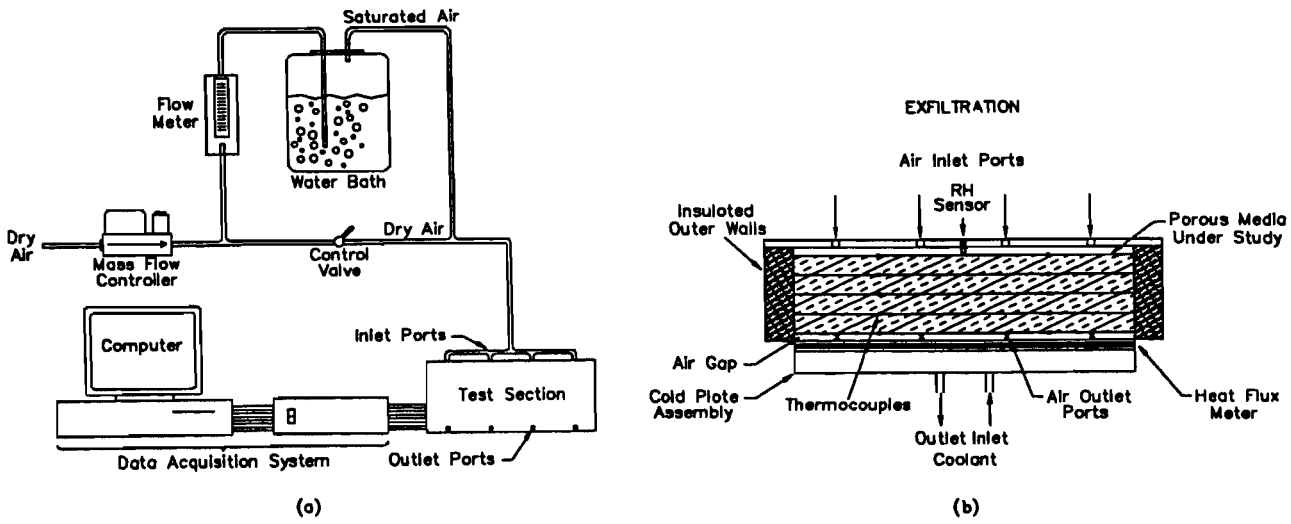

Figure 11: A schematic of (a) the experimental apparatus and (b) the details of the test section.

field throughout the slab. A single thermocouple is placed in the air gap between the insulation and the cold plate to measure the temperature of the air as it flows out of the apparatus. A relative humidity sensor is placed in the upper portion of the apparatus to measure the RH of the air passing through the sample. The upper surface of the slab is exposed to the direct exfiltration of moist air at room temperature, which can be controlled at various relative humidities and volumetric flow rates. The volumetric flow rate is set using a 1-20 L/min ($1.67 \cdot 10^{-5}$-$3.33 \cdot 10^{-4}$ m^3/s) mass flow controller. The test section is also designed to allow for the future implementation of infiltration tests; i.e., air can flow from the cold side to the warm side of the insulation slab. The edges of the glass- fiber slab are insulated by polystyrene boards to minimize the edge heat loss, and the underside of the plate covering the top apparatus has been coated with aluminum foil to minimize radiation effects.

Each layer of the glass-fiber slab is initially dried in an oven at 105 °C for about 15 hours, and then they are wrapped individually in plastic sheets and allowed to cool to room temperature (approximately 21 °C). When the samples have cooled and each layer has been weighed, they are mounted one at a time in the apparatus. Data are recorded for an initial period of 5 minutes before the flow of moist air starts and before the coolant in the heat exchanger is supplied to cool the cold plate. Once these two mechanisms have been engaged, the temperature of the cold plate and the relative humidity of the air entering the experiment stabilize within 15 to 20 minutes. The temperatures of the glass-fiber slab, cold plate and air leaving the apparatus are recorded and monitored by a microcomputer through a data acquisition unit. A typical experiment runs from 1 to 3 hours which covers both a transient and quasi-steady-state period. At the end of each test, the slab is taken out of the apparatus and each layer is weighed using an electronic scale, to determine the amount and distribution of moisture/frost during that period of time. Simultaneously, 7 small disks,

Table 1 The Experimental Conditions and the Properties of the Glass-fiber Slab

T_∞	°C	20.0 ± 1.0
T_c	°C	-20.0 ± 1.0
ϕ_∞		$0.60 \sim 0.90 \pm 0.02$
$\dot{V}$	m^3/s	$1.66 \cdot 10^{-4} \sim 2.49 \cdot 10^{-4}$ $\pm 1\%$
ϵ		0.98
ρ (dry)	kg/m^3	52.0
k_{eff} (dry)	W/m-K	0.030
L	m	0.10 (0.985 inch × 4)

which are embedded into the top of the cold plate, are removed and weighed. This is done to determine the amount of frost growth on the cold plate, which is used in the heat balance for calculating the heat flux through the insulation slab.

From the experiments, the time variation of the temperature field in the slab, the time variation of the heat flux at the cold side of the slab, and the moisture/frost accumulation can be found for various air exfiltration velocities and relative humidities. The conduction heat flux at the cold side of the insulation slab (see Fig. 11b) can be derived from the following energy balance equation:

$$Q_L = \frac{1}{A}(AQ_c + \dot{m}c_{pa}\Delta T\dot{m}_f h_{sg}) \tag{16}$$

where A is the surface area of the cold plate which is the same as the slab cross section area, Q_c is the heat flux measured by the heatflux meter on the cold plate, and $\dot{m}$ is the measured airflow rate, ΔT is the temperature difference between the measured cold surface temperature of the fiberglass slab and the measured temperature of air leaving the air gap, and $\dot{m}_f$ is the average rate of frost mass accumulation on the cold plate, which is obtained from the measured frost mass at the end of the test, divided by the test duration.

The uncertainty in the heat-flux meter measurement is estimated within 6%. All thermocouples are calibrated using a standard calibrator and the uncertainty in temperature measurement is within 0.1 °C. The relative humidity is within 2% and the electronic scale is accurate to 0.2 grams. Table 1 gives the range of experimental conditions and the basic properties of the glass-fiber slab used.

4.2 Experimental results

The temperature distribution, heat flux and moisture accumulation for a typical test condition, ($\dot{V} = 1.66 \cdot 10^{-4}$ m^3/s, $u_g = 1.0$ mm/s at z=0, $T_\infty = 21$ °C, $T_c = -19$ °C, $\phi_\infty = 0.90$), is shown in Figs. 12 to 14. For the test sepcimen thickness, L, of 10 cm the transient time for air flow from $z = 0$ to $z = L$ is 1.67 min for $u_g = 1.0$ mm/s at $z = 0$. In Fig. 12, the temperatures at the top, middle and bottom of the fiberglass slab, in the bottom air gap and of the cold plate are shown as a function of testing time. During the initial transient

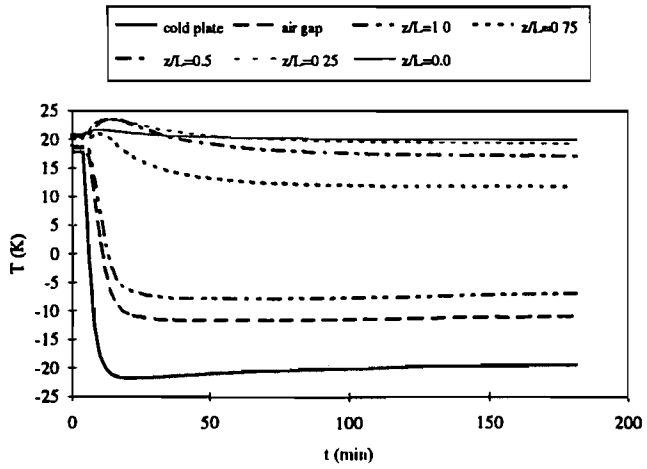

Figure 12: Time variation of the measured temperatures at various locations: $\dot{V} = 1.66 \times 10^{-4}$ m^3/s ($u_g = 1.0$ mm/s) and $\phi_\infty = 0.90$.

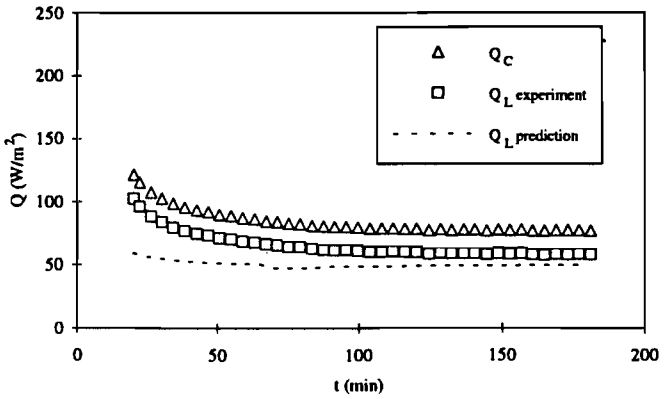

Figure 13: Time variation of the measured heat fluxes across the cold plate and at the cold side of the slab: $\dot{V} = 1.66 \times 10^{-4}$ m^3/s ($u_g = 1.0$ mm/s) and $\phi_\infty = 0.90$.

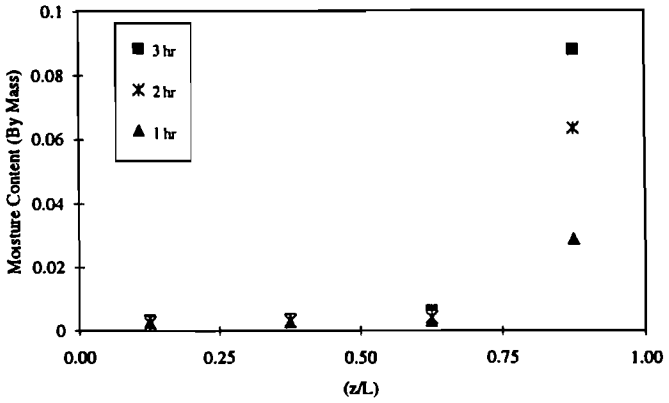

Figure 14: Distributions of the measured total moisture accumulation for different times: $\dot{V} = 1.66 \times 10^{-4}$ m^3/s ($u_g = 1.0$ mm/s) and $\phi_\infty = 0.90$.

period, a strong adsorption effect can be seen as the temperature in the top half of the slab rises and is higher than the ambient temperature. This phenomenon is similar to the test under no exfiltration as reported in [5]. Because the slab is initially dried in the oven, the sudden exposure to a moist air flow at RH =90% results in a strong energy release due to the adsorption of water vapor onto the glass fiber surfaces. It is interesting to see from Fig. 12 that the adsorption strongly affects the temperature in the middle of the slab, while in the vapor diffusion-only process yet under the similar temperature and relative humidity boundary conditions, the adsorption effect is only detected at the locations near the top surface of the slab [5]. This is because, in the exfiltration test, the downward air movement within the slab causes the dry region to be larger than that in the diffusion- only test so that the adsorption can take place in a relatively large domain.

Fig. 13 shows the time variation of the measured heat fluxes on the cold plate, Q_c, and at the cold surface of the slab, $Q_{\rm L}$, obtained using equation (1). After the initial transient period (about 20 minutes after the coolant supplied to the cold plate heat exchanger), the heat flux, Q_c, gradually decreases and reaches a quasi-steady state at about two hours. In general, Q_c is approximately 20 % higher than $Q_{\rm L}$, the heat flux leaving the cold surface of the insulation slab. This is because the measured heat flux on the cold plate includes the latent heat due to the frost growth and the air enthalpy deficit. The total heat transported from the inside of the slab to $z = L$ (equal to Q_L plus air enthalpy flow) is transferred to the cold plate by radiation and convection. For this test case, if we assume that the emissivity for both frost and fiberglass surfaces is close to unity and the frost surface temperature is nearly the same as the cold plate temperature, the radiation heat flux is estimated about one third of the heat flux measured on the cold plate. This is consistent with the experimental observation that a significant frost layer is developed on the cold plate for the test results

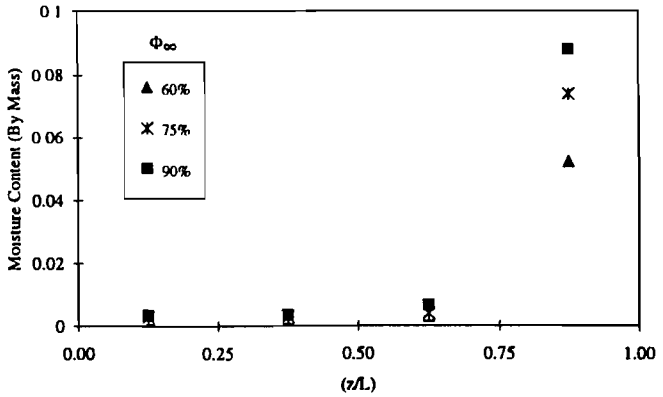

Figure 15: Distributions of the measured total moisture accumulation for different air inlet relative humidities: $\dot{V} = 1.66 \times 10^{-4}$ m^3/s ($u_g = 1.0$ mm/s) and $t = 3$ hr.

shown in Fig. 13, as a result of radiation heat transfer and moisture transport, among other effects.

It is shown in Fig. 14 for the same test condition as in Fig. 13, the moisture accumulation in the slab mainly concentrates near its cold side (each data point represents the average for each slab layer). The moisture content in the bottom layer increases significantly with time. This trend is similar to the test results with no exfiltration [7], but contrary to the numerical results by Tien and Vafai [8]. This may be chiefly due to the fact that the time duration for moisture accumulation in Tien and Vafai's numerical results is much shorter than in our tests. In ref. [5], it was also found that during the initial period, more moisture accumulates near the warm side of the insulation slab while later more moisture (frost) is found near the cold side of the slab. It should be noted that for the operating temperature above the freezing point the moisture accumulation is not significant even with infiltration/exfiltration; e.g., an order of 10^{-4} in the liquid volume fraction was reported in [8] . With frosting, however, the exfiltration effect on the moisture accumulation is more pronounced; moisture content reaches 0.09 (by mass), or about $7 \cdot 10^{-3}$ (by volume). Similar trends are seen for other inlet air relative humidities. In general, the resulting moisture/frost accumulation in the bottom layer increases as the air inlet relative humidity increases (Fig. 15). As a consequence of the increase in moisture/frost accumulation, the heat loss through the insulation slab will also increase. As shown in Fig. 16, the quasi-steady-state heat flux increases with ϕ_∞ for the given exfiltration rate, and also increases with the exfiltration rate for the given ϕ_∞. It can be seen that for otherwise the same conditions, increasing the exfiltration rate will result in more significant increase in the heat loss than increasing the ambient relative humidity could do.

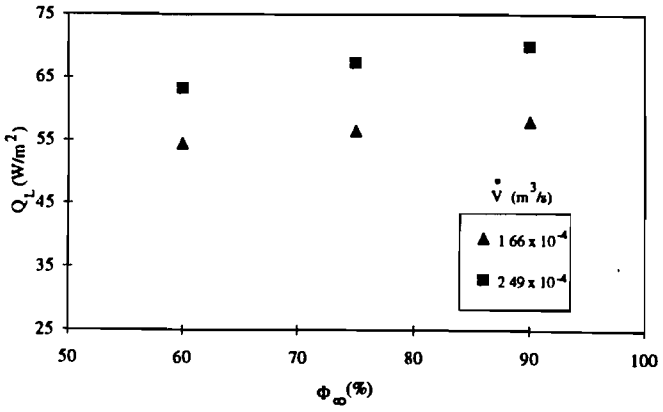

Figure 16: Measured quasi-steady-state heat flux at the cold side of the slab as a function of ϕ_∞ and $\dot{V}$: $t = 3$ hr.

5 NUMERICAL SIMULATION OF EXFILTRATION IN INSULATION UNDER A THERMAL GRADIENT

The following one-dimensional, transient analysis of simultaneous heat and mass transfer in insulation with phase changes is based on the model in ref. [5]. The modification is made to include the momentum equation for gaseous phases. The physical mechanisms involved in the vapor mass transfer are then the creeping flow for gaseous phases (air and water vapor) and vapor diffusion. For heat transfer, both conduction and convection occur. The major assumptions are (a) all phases in the porous medium are in local thermodynamic equilibrium, (b) the pressure gradient in the slab is uniform and equal to the total pressure drop across the slab divided by the slab thickness, and (c) accumulated frost exist only as isolated ice crystals [5]. The schematic of this model is depicted in Fig. 17. It is shown that any moisture that might be accumulated in the insulation is transported from the ambient air through both air movement and vapor diffusion under a thermal gradient. Assumption (b) is imposed for the simplification of the physical problem. This is justified provided that the moisture/frost accumulation is not very large so that the local pore-level structure is not changed significantly. Although an alternative with respect to assumption (b) could be to assume the constant Darcy velocity in the slab, assumption (b) is thought to be more appropriate to the experimental conditions in this study.

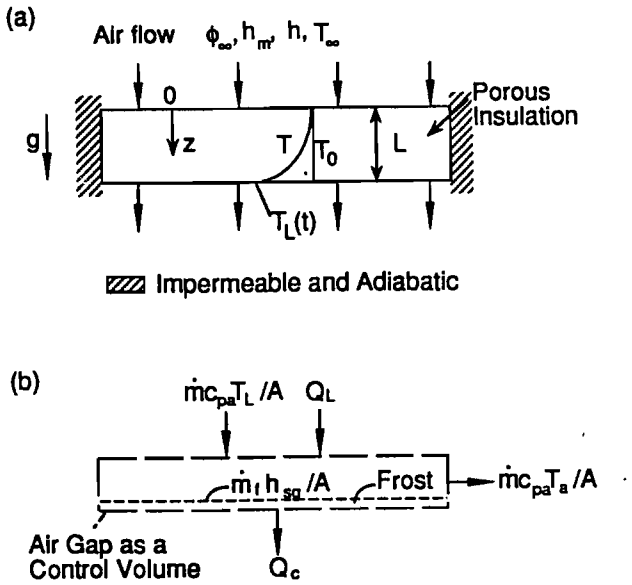

Figure 17: Transient condensation and frosting in an insulation slab with (a) prescribed boundary conditions and (b) the air gap condition adjacent to the cold plate.

5.1 Governing Equations

The coupled, non-linear partial differential equations below are used to describe the transport phenomena.

Liquid/ice phase continuity equation:

$$\frac{\partial \epsilon_l}{\partial t} + \frac{\dot{m}}{\rho_l} = 0 \tag{17}$$

Gas momentum equation:

$$u_g = -\frac{K_g \epsilon_g}{\mu_g}\left(\frac{\partial (p_g - p_o)}{\partial z} - \rho_g g\right) \tag{18}$$

Gas diffusion equation:

$$\frac{\partial (\epsilon_g \rho_{cg})}{\partial t} + \frac{\partial (\rho_{cg} u_g)}{\partial z} - \dot{m} = \frac{\partial}{\partial z}\left(D_{\text{eff}} \frac{\partial \rho_{cg}}{\partial z}\right) \tag{19}$$

Energy equation:

$$\rho c_p \frac{\partial T}{\partial t} + \rho_g c_{pg} u_g \frac{\partial T}{\partial z} + \dot{m}\,\Delta h = \frac{\partial}{\partial z}\left(k_{\text{eff}} \frac{\partial T}{\partial z}\right) \tag{20}$$

where ρ_l in equation (18) refers to the ice phase for the frozen region, and Δh in equation (5) is the heat of condensation for the wet region, the heat of sublimation for the frozen region, or the heat of adsorption for the dry region. $\dot{m}$ is the dimensionless mass rate of phase change per unit volume.

5.2 Supplementary Equations and Boundary Conditions

Additional equations used are:
Volumetric constraint:

$$\epsilon_s + \epsilon_l + \epsilon_g = 1 \tag{21}$$

Thermodynamic relations:

$$p_{ng} = p_t - p_{cg} \tag{22}$$

$$p_{ng} = R_{ng}\rho_{ng}T \tag{23}$$

$$p_{cg} = R_{cg}\rho_{cg}T \tag{24}$$

and for saturation conditions

$$p_{cg} = p_{ref} \exp\left[-\frac{\Delta h}{R_{cg}}\left(\frac{1}{T} - \frac{1}{T_{ref}}\right)\right] \tag{25}$$

where

$$\rho = \epsilon_s\rho_s + \epsilon_l\rho_l + \epsilon_g(\rho_{cg} + \rho_{ng}) \tag{26}$$

$$c_p = \frac{\epsilon_s\rho_s c_s + \epsilon_l\rho_l c_l + \epsilon_g(c_{cg}\rho_{cg} + c_{ng}\rho_{ng})}{\rho} \tag{27}$$

$$k_{eff} = \epsilon_s k_s + \epsilon_l k_l + \epsilon_g k_g \tag{28}$$

Note that in equation (28) the dispersion effect on the effective thermal conductivity is not included due to the lack of sufficient information. For the dry region, the BET equation (14) [5] is used to calculate the rate of adsorption.

In the above formulation, the unknown variables are T, ρ_{cg}, ρ_{ng}, ϵ_l, ϵ_g, $\dot{m}$, p_{ng}, p_{cg}, and u_g while all the transport and thermophysical properties for the individual phases are known from empirical data. Equations (2) – (10) can then be used to solve for these nine unknowns if the phase changes are due to condensation and frosting. If the adsorption occurs in the dry region of the slab, equation (10) is replaced by equation (14).

The boundary and initial conditions are depicted in Fig. 17. Mathematically, they can be expressed as follows.

$$\frac{\partial T(z=0,t)}{\partial z} = -h[T_\infty - T(z=0,t)], \tag{29}$$

$$\frac{\partial \rho_{cg}(z=0,t)}{\partial z} = -h_m[\rho_\infty - \rho_{cg}(z=0,t)], \tag{30}$$

$$T(z=L,t) = T_L(t), \tag{31}$$

$$\frac{\partial \rho_{cg}(z=L,t)}{\partial z} = 0, \text{ when } \phi < 1,$$
$$\rho_{cg}(z=L,t) = \rho_s, \text{ when } \phi = 1, \tag{32}$$

$$T(z,t=0) = T_0, \tag{33}$$

$$\rho_{cg}(z, t = 0) = \phi_0 \rho_s(T(z, t = 0)), \tag{34}$$

$$\epsilon_\beta(z, t = 0) = \epsilon_{\beta 0}(z), \tag{35}$$

where in equation (31) $T_L(t)$ is obtained from the measured temperature data. The temperature boundary condition at $z = L$ is governed by the radiation heat transfer between the bottom surface of the insulation slab and the frost surface on the cold plate (Fig. 17b) in addition to convection heat transfer in the air gap. However, due to the difficulties in obtaining the frost surface temperature and the uncertainty in the emissivity data for both fiberglass and frost surfaces, the specification of the radiation and convection boundary conditions at $z = L$ is not adopted in the present study.

The finite difference forms of Eqs. (2) to (5) are derived using the implicit scheme with the backward difference for the time derivative. The central difference form is used for internal nodes and the backward or forward difference is used for boundary nodes. The convection term in equation (5) is discretized using the first-order difference (downwind scheme) to stabilize the iteration procedure. The under-relaxation scheme is used in the iteration.

5.3 Comparison of the Prediction with the Experimental Results

The prediction, based on the model presented above, is shown in Fig. 18. The comparison between the measured and predicted temperature inside the slab is generally favorable (Fig. 18a). In Fig. 18(b), the predicted moisture content is higher than the measured ones at about top half of the slab, while the prediction is lower than the measured moisture content near the cold side of the slab. Note that adsorption occurs in the warm part of the slab, thus the uncertainty in the adsorption characteristics of fiberglass (i.e., using a simplified BET equation) contributes to the discrepancy between the prediction and measured data. Near the cold side, a significant frost growth could occur on the bottom surface of the test slab due to radiation heat losses not fully accounted for in the model. This phenomenon is not included in the simplified boundary conditions at $z = L$. Similar conclusion can also be drawn from Fig. 14, where the predicted heat flux, Q_L, is shown to be lower than the measured data. Recall that Q_L is defined at $z = L$; therefore, including frost growth at $z = L^+$ would add the phase change contribution to Q_L.

A comparison, based on the numerical simulation, between the quasi-steady-state conduction heat flux, Q_L, for a given exfiltration condition and the heat flux, Q'_L, for the same boundary and initial conditions but without air movement in the insulation is listed in Table 2. Both Q_L and Q'_L are defined as $-(k_{\text{eff}} \partial T/\partial z)_{z=L}$. The heat-flux ratio, Q_L/Q'_L is in the vicinity of 3.30 for three inlet air relative humidities. Although further validation by experiment is needed, this conclusion is consistent with the study by Tien and Vafai [7]; i.e., the even small pressure drop across the insulation slab can result in a significant heat loss. This increase in conduction heat loss is due partly to the convection and internal latent heat release from moisture condensation or frosting, which alters the temperature field, and partly to the increase in the thermal conductivity as a result of the increase in the moisture content. This result can also be seen by comparing the conduction heat flux at the warm side

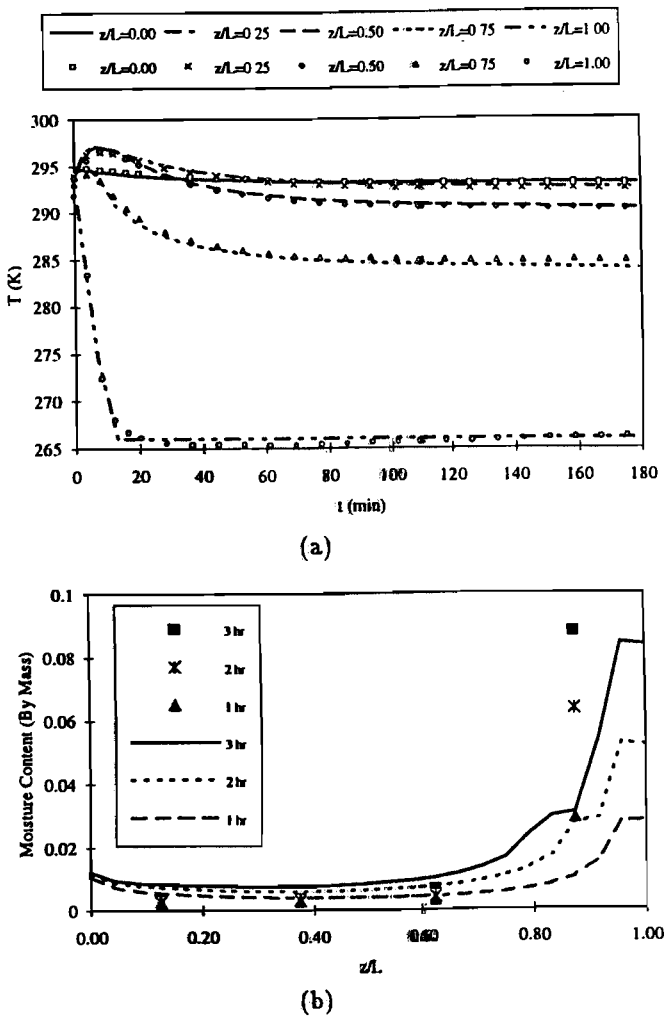

Figure 18: Comparison of the predicted (a) temperature and (b) moisture content (lines) with the measured data (points): $\dot{V} = 1.66 \times 10^{4}$ m^3/s ($u_g = 1.0$ mm/s) and $\phi_\infty = 0.90$.

Table 2 Predicted quasi-steady-state heat fluxes: $Q_L(z = L)$ and $Q_o(z = 0)$ (with the exfiltration effect), $Q'_L(z = L)$ (without exfiltration), and the total sensible heat exchange per slab area, Q_{cv}; $\dot{V} = 1.66 \times 10^{-4}$ m^3/s ($u_g = 1.0$ mm/s) and $t = 3$ hr.

ϕ_∞, %	Q_L, W/m^2	Q_o, W/m^2	Q_{cv}, W/m^2	Q'_L, W/m^2	Q_L/Q'_L	Q_L/Q_o	$Q_{cv}/(Q_L - Q_0)$
60	39.17	1.36	28.37	12.55	3.12	28.8	0.75
75	44.72	1.09	28.43	13.60	3.29	41.0	0.65
90	49.74	0.32	28.61	14.66	3.39	155.4	0.58

of the insulation slab (i.e., z=0), Q_o, with Q_L, as presented in Table 2. Q_L/Q_o is about 155 for $\phi_\infty = 0.9$. Again, the difference between Q_L and Q_o is accounted for by both convection heat transfer and the rate of heat release due to the phase change of water vapor within the insulation slab. We estimate the total sensible heat transfer in the slab per unit area using the following equation,

$$Q_{cv} = \rho_a c_p \frac{\dot{V}}{A}(T_0 - T_L), \tag{36}$$

and compare Q_{cv} with $Q_L - Q_o$. We may conclude, from Table 2, that the convection inside the insulation slab contributes 58 % to the heat loss at $z = L$ for $\phi_\infty = 90\%$ and the remaining 42 % is due to the latent heat release during moisture and frost accumulation. It should be noted that for the three simulation runs shown in Table 2 (for different ϕ_∞), the same $T_L(t)$ is used in order to test the sensitivity of ϕ_∞. In experiments, however, the temperature of the cold plate, T_c, was controlled at the same value; therefore, changing ϕ_∞ results in a change in T_L on the cold bottom side of the insulation because of different frost accumulation on the cold plate and cold side of the insulation slab. It is thus shown, from Table 2, that given the same T_L, the latent heat decreases with ϕ_∞ as a result of the decrease in moisture/frost accumulation. For $\phi_\infty = 0.75$, $Q_{cv}/(Q_L - Q_o)$ is equal to 0.65, which means the latent heat contributes 35 % to the heat transfer at $z = L$.

6 SUMMARY

Thermal hysteresis has been defined by the differences between the adsorption and desorption isotherms and between heats of adsorption and desorption. New data is presented for the desorption process which is contrasted with previously obtained adsorption data. The significance of this phenomenon and its interaction with dynamic heat and mass transport processes such as that a building insulation undergoes are investigated through experiments and a numerical simulation. Based on the above discussion the following conclusions may be drawn within the scope of heat and mass diffusion processes:

(a) From the measurement of heat of desorption reported here and data for the heat of adsorption, the thermal hysteresis phenomenon clearly exists for typical commercial fiberglass insulation.

(b) During transient processes thermal hysteresis effects are pronounced regardless of whether the insulation slab is initially dry or wet and above or below freezing temperature.

(c) Neglecting thermal hysteresis effects in simulating a dynamic transport process can lead to errors in the instantaneous heat flux of up to 51% for an initially dry fiberglass slab and 23% for an initially moist slab.

An experimental apparatus was reported and allows for the investigation of exfiltration and infiltration effects on the heat and moisture transport in insulation materials under the controlled test conditions. The preliminary test results for exfiltration tests (winter condi-

tions but excluding the buoyancy effects) were presented for a given temperature difference across a fiberglass test slab ($T_c = 20 \pm 1$ °C and T_∞=21 °C) at various air relative humidities (60 to 90 % RH) and two different exfiltration rates (1.66×10^{-4} and 2.49×10^{-4}m^3/s, or $u_g = 1.0$ and 1.5 mm/s). In this range, it is found that the increase in moisture accumulation under frosting condition could be an order of magnitude higher than for the temperature range above freezing. A one-dimensional numerical model predicted simultaneous heat transfer, vapor diffusion, convection, phase change and adsorption effects. Predicted results agree favorably with the measured data. Preliminary results show that the conduction heat loss at the cold side of the insulation slab can be typically up to 300% higher with air exfiltration, as compared to the moisture diffusion-only process (i.e., no exfiltration) under the same temperature boundary condition.

7 FUTURE WORK

These experimental and numerical studies of one-dimensional transient heat, moisture and air diffusion and transport in fiberglass insulation, presented in the studies reported this year and previously, clearly illustrate a wide range of physical phenomena including adsorption/desorption, thermal hysteresis, condensation/evaporation, sublimation/ablimation, heat transfer, and air infiltration/exfiltration. The errors that could result by various simplified models have been shown to be very significant. Nonetheless, more work should be done to illustrate these phenomena and the size of errors that could result through the use of simplified models for various insulated structures under typical ranges of operating conditions. These studies should include:

1. The range of typical materials used in wall and ceiling structures including wood, dry wall, air-vapor retarders and various insulation materials. (It is expected that these various materials will give use to a wide range of transient time constants for both heat and moisture transfer. Some of these, like for moisture transfer through wood, will be much larger than the diurnal cycle times.)

2. Although transient, one-dimensional studies were presented in the results, two- and three- dimensional heat, moisture and air transport and diffusion should be investigated. (These could all differ somewhat from a given insulated structure with various boundary conditions. Furthermore, the importance of two- and three- dimensional heat and moisture transfer effects will themselves vary with the dynamics of the initial and boundary conditions. Particular attention must be given to two- and three- dimensional air infiltration/exfiltration because it is expected that most of this air flow takes place through cracks and holes in the air-vapor retarders.) The above studies should be, by their very nature, comprehensive and intensive, and the results will be complex and difficult to use in the design of the more highly insulated buildings of the future. That is, although simplified models of heat and moisture transfer in the more lightly insulated buildings have been used very increasingly in the past, the significance of modeling errors and the physical deterioration of insulated structures over

time are expected to increase with the amount of insulation and the cost of energy and construction.

3. It will, therefore, be necessary to delineate the physical and thermal deterioration of insulation materials and the errors incurred with various simplified design models.

4. Finally, more complex design models will be necessary for structures subjected to a wide range of conditions, similar to those investigated here.

The recent literature on building envelopes and behaviors of porous insulation clearly indicates that all four of these activities are being actively pursued. What remains to be done is to incorporate the latest porous material characteristics such as those discussed in this report. Including the phenomena reported here will add considerably to the complexity of these studies.

8 NOMENCLATURE

A	cross-section area of the slab perpendicular to the main airflow, m^2
C	empirical constant in equations (14)
c_p	heat capacity at constant pressure, J/kg-K
D_{eff}	effective vapor diffusivity, m^2/s
Fo	Fourier number, $\alpha_{\text{eff}} t/L^2$
h	heat transfer coefficient, W/m^2-K
h_m	mass transfer coefficient, m/s
Δh	heat of phase change, J/kg
k	thermal conductivity, W/m-K
L	characteristic length of the slab, m
$\dot{m}$	rate of phase change, kg/m^3-s
p	pressure, Pa
Q	heat flux, W/m^2
R	gas constant, J/kg-K
t	time, s
T	temperature, K
u	velocity, m/s
$\dot{V}$	exfiltration rate, m^3/s
W	percentage water content by weight, %
z	coordinate axis, m

Greek Symbols

α	thermal diffusivity, m^2/s
ϵ	volume fraction
ϕ	relative humidity
ρ	density, kg/m^3
τ	percentage of bonding material

Subscripts

a	air
c	cold
cg	condensable phase
f	frost
g	gas phase which consists of air and water vapor
l	liquid phase in wet region or ice phase in frozen region
L	at $z = L$
ng	non-condensable phase
o	at $z = 0$
ref	reference point
s	solid phase
t	total
tr	transition
v	vapor phase
β	liquid or ice phase
γ	gas phase which consists of air and water vapor
σ	solid phase
∞	ambient

9 REFERENCES

1. C. J. Simonson, Y.-X. Tao, and R. W. Besant, Thermal hysteresis in a fibrous insulation, accepted by *Int. J. Heat Mass Transfer* (1993).

2. Y.-X. Tao, and D. R. Mitchell, and R. W., Effects og exfiltration on moisture and frost accumulation in a fibrous insulation, the Sixth International Symposium on Transport Phenomena in Thermal Engineering, Seoul, Korea, May 9-13, 1993.

3. S. G. Gregg, and K. S. Sing, K. S. W., *Adsorption, Surface Area and Porosity*, Academic Press, London, p. 17 (1982).

4. Y.-X. Tao, R. W. Besant, and C. J. Simonson, Measurement of the heat of adsorption for a typical fibrous insulation, *ASHRAE Trans.* **98**, Pt. 2 (1992).

5. Y.-X. Tao, R. W. Besant, and K. S. Rezkallah, The transient thermal response of a glass-fiber insulation slab with hygroscopicity effects, *Int. J. Heat Mass Transfer* **35**, 1155-1167 (1992).

6. Y.-X. Tao, R. W. Besant, and K. S. Rezkallah, Modeling of frost formation in a fibrous insulation slab and on an adjacent cold plate, *Int. Comm. Heat Mass Transfer* **18**, 609-618 (1991).

7. K. Vafai, and S. Sarkar, Condensation effects in a fibrous insulation slab, *J. Heat Transfer* **108**, 667-675 (1986).

8. H. C. Tien, and K. Vafai, A synthesis of infiltration effects on an insulation matrix, *Int. J. Heat Mass Transfer.* No. 33, pp. 1263-1280 (1990).

10 APPENDIX

The governing differential equations used for studying simultaneous heat and mass diffusion with thermal hysteresis effects in fiberglass insulation (section 2) are:

β phase continuity equation:

$$\frac{\partial \epsilon_\beta}{\partial t} + \frac{\dot{m}}{\rho_\beta} = 0 \tag{37}$$

Gas diffusion equation:

$$\frac{\partial(\epsilon_\gamma \rho_v)}{\partial t} - \dot{m} = \frac{\partial}{\partial z}(D_{eff} \frac{\partial \rho_v}{\partial z}) \tag{38}$$

Energy equation:

$$\rho c_p \frac{\partial T}{\partial t} + \dot{m}\, \Delta h = \frac{\partial}{\partial z}(k_{eff} \frac{\partial T}{\partial z}) \tag{39}$$

where the subscript β denotes the liquid phase for $T > 0°C$ and the ice phase for $T \leq 0°C$, and Δh means the latent heat which can be either the enthalpy of condensation, enthalpy of ablimation, or enthalpy of adsorption, depending on the local physical conditions. The algebraic equations of constraint are:

Volumetric constraint:

$$\epsilon_\sigma + \epsilon_\beta + \epsilon_\gamma = 1 \tag{40}$$

Thermodynamic relations:

$$p_a = p_t - p_v \tag{41}$$

$$p_a = R_a \rho_a T \tag{42}$$

$$p_v = R_v \rho_v T \tag{43}$$

and for saturation conditions

$$p_v = p_0 \exp\left[-\frac{\Delta h}{R_v}\left(\frac{1}{T}\frac{1}{T_{ref}}\right)\right] \tag{44}$$

where

$$\rho = \epsilon_\sigma \rho_\sigma + \epsilon_\beta \rho_\beta + \epsilon_\gamma(\rho_v + \rho_a) \tag{45}$$

$$c_p = \frac{\epsilon_\sigma \rho_\sigma c_\sigma + \epsilon_\beta \rho_\beta c_\beta + \epsilon_\gamma(c_v \rho_v + c_a \rho_a)}{\rho} \tag{46}$$

$$k_{eff} = \epsilon_\sigma k_\sigma + \epsilon_\beta k_\beta + \epsilon_\gamma \frac{k_v \rho_v + k_a \rho_a}{\rho_v + \rho_a} \tag{47}$$

The dimensionless heat flux is defined as

$$Q' = \frac{\left(k_{eff}\frac{\partial T}{\partial z}\right)_{z=L}}{\left(k_{\rm dry}\frac{\partial T}{\partial z}\right)_{z=L,{\rm dry}}}. \tag{48}$$

The boundary and initial conditions are:

$$k_{eff}\frac{\partial T(z=0,t)}{\partial z} = -h_a[T_\infty - T(z=0,t)], \tag{49}$$

$$D_{eff}\frac{\partial \rho_v(z=0,t)}{\partial z} = -h_m[\rho_\infty \rho_v(z=0,t)], \tag{50}$$

$$T(z=L,t) = T_c, \tag{51}$$

$$\frac{\partial \rho_v(z=L,t)}{\partial z} = 0. \tag{52}$$

$\rho_v = \rho_s$, employing Clapeyron equation, will replace the above equation when $\rho_v(z=L,t)$ reaches the saturated value.

$$T(z,t=0) = T_0, \tag{53}$$

$$\rho_v(z,t=0) = \phi_0 \rho_s(T(z,t=0)), \tag{54}$$

$$\epsilon_\beta(z,t=0) = \epsilon_{\beta 0}(z). \tag{55}$$